

See discussions, stats, and author profiles for this publication at: <https://www.researchgate.net/publication/272079855>

Effect of the Polymer Concentration on the Rayleigh-Instability-Type Transformation in Polymer Thin Films Coated in the Nanopores of Anodic Aluminum Oxide Templates

ARTICLE *in* LANGMUIR · FEBRUARY 2015

Impact Factor: 4.46 · DOI: 10.1021/la504901h · Source: PubMed

CITATIONS

2

READS

17

2 AUTHORS, INCLUDING:



Jiun-Tai Chen

National Chiao Tung University

58 PUBLICATIONS 1,076 CITATIONS

SEE PROFILE

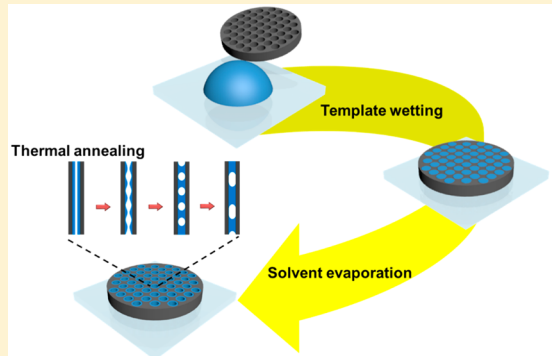
Effect of the Polymer Concentration on the Rayleigh-Instability-Type Transformation in Polymer Thin Films Coated in the Nanopores of Anodic Aluminum Oxide Templates

Chia-Chan Tsai and Jiun-Tai Chen*

Department of Applied Chemistry, National Chiao Tung University, Hsinchu 30010, Taiwan

 Supporting Information

ABSTRACT: We study the Rayleigh-instability-type transformation of polystyrene (PS) thin films coated in the nanopores of anodic aluminum oxide (AAO) templates. The PS thin films are fabricated using a solution-wetting method, in which the wall thicknesses are controlled by the concentrations of the polymer solutions and the diameters of the nanopores. By thermal annealing, the surfaces of the thin films undulate and the morphologies transform from nanotubes to Rayleigh-instability-induced nanostructures (short nanorods) and long nanorods. To understand the mechanism of the morphology transformation further, we construct the morphology diagrams by annealing the PS thin films at different temperatures and times. We observe that the morphology diagrams of the PS thin films prepared by different concentrations are similar, indicating that the transformation kinetics are not affected by the film thicknesses. The values of the undulation wavelengths, however, are controlled by the film thicknesses and the diameters of the nanopores.



INTRODUCTION

In recent years, polymer nanomaterials have attracted great attention for not only their unique properties but also their applications in areas such as sensors, transistors, drug deliveries, and photovoltaic cells.^{1–5} The shapes and morphologies of polymer nanomaterials are critical for their properties and applications. One of the widely used methods to fabricate polymer nanostructures is the template method.^{1,6–10} Polymers are infiltrated into the nanopores of porous templates, and the sizes of the polymer nanostructures can be controlled by the sizes of the nanopores of the templates.^{11–13} The porous templates are used only as scaffolds that can be removed selectively. The anodic aluminum oxide (AAO) template, prepared by the anodization of aluminum foils, is one of the commonly used templates.^{14–17} The pore sizes and interpore distances of the AAO templates can be controlled by the anodization conditions and pore-widening processes.^{18,19}

In 2007, Russell et al. investigated the morphology transformation of poly(methyl methacrylate) (PMMA) thin films coated in the nanopores of AAO templates driven by the Rayleigh instability.²⁰ They discovered that hierarchical polymer nanorods with encapsulated air bubbles can be formed after thermal annealing.^{20,21} Recently, we also studied similar transformation phenomena by thermal annealing polystyrene (PS) thin films coated in the nanopores of AAO templates.²² PS samples with two different molecular weights ($M_w = 24$ and 100 kg/mol) were used, and the morphology diagrams of the PS nanostructures at different stages were also constructed. Slower kinetics of the morphology transformation were

observed for PS polymers with higher molecular weights, because of their lower mobilities.²²

Despite these works, many factors on the behaviors of the Rayleigh-instability-type transformation of polymer thin films confined in cylindrical nanopores, however, are still not understood. The thermal dynamics and kinetics of the transformation processes are related to many factors, such as the type of polymer, the polymer concentration, the annealing condition, and the interaction between the wall and the polymer. One of the major questions is whether the morphology diagrams of the polymer nanostructures are affected by the polymer concentration. In addition, it is also unclear about the relationship between the undulation wavelengths and the diameters of the nanopores using different polymer concentrations.

To address these issues, in this work, we prepare polymer thin films confined in the nanopores of AAO templates using PS solutions with different polymer concentrations. The wall thicknesses of the polymer thin films are controlled by both the polymer concentrations and the diameters of the nanopores. The morphologies of the confined polymer thin films annealed at different temperatures and times are examined by scanning electron microscopy (SEM). Morphology diagrams of the samples annealed at different conditions are also constructed to elucidate the kinetics of the morphology transformation process.

Received: December 17, 2014

Revised: February 4, 2015

Published: February 5, 2015

driven by the Rayleigh instability. The introduction of the Rayleigh instability and the related equations are discussed in the Supporting Information.^{23–28}

In this work, we study the Rayleigh instability of PS thin films confined in the nanopores of AAO templates using different polymer concentrations. As shown in Figure 1, there are four

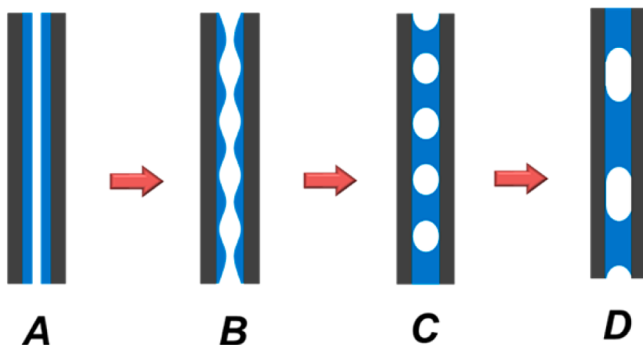


Figure 1. Graphical illustration of the Rayleigh-instability-driven transformation of polymer nanotubes confined in the nanopores of AAO templates. After thermal annealing, the polymer nanotubes (A) transform to undulated structures (B), Rayleigh-instability-induced structures (C), and nanorods (D).

different morphologies in the transformation process, including nanotubes (A), undulated structures (B), Rayleigh-instability-induced structures (C), and nanorods (D), according to the works by Russell et al., Jin et al., and our group.^{20–22,29} The Rayleigh-instability-induced structures (C) are short nanorod structures with encapsulated air bubbles.

To investigate the effect of the polymer concentration on the transformation process, PS with five different concentrations (1, 3, 5, 10, and 20 wt %) is used. The morphology diagrams of the polymer nanostructures at different annealing conditions are constructed, and similar morphology diagrams are obtained for the samples prepared using different polymer concentrations. This result indicates that the transformation kinetics are not affected by the thicknesses of polymer films at the same pore diameters. To clarify the transformation process further, we also perform quantitative studies on the relationships between the undulation wavelengths and the tube radii for the samples prepared by different polymer concentrations. We find that the undulation wavelengths are determined by the radii of the air cylinders. Therefore, at a lower polymer concentration, the radii of the air cylinders are larger at a given pore diameter, resulting in smaller discrepancies of the data from the theoretical values at the polymer concentration of 0 wt %.

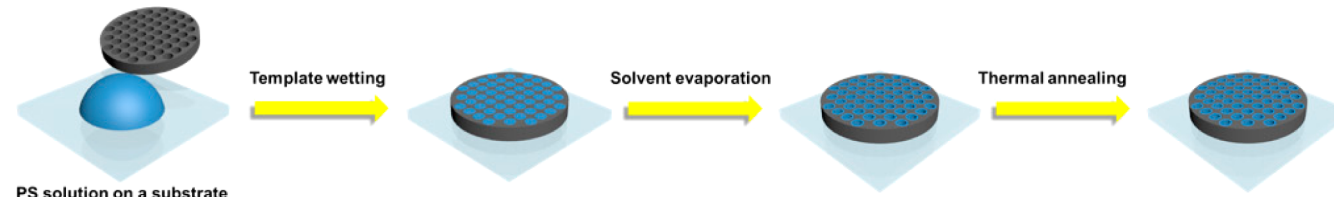


Figure 2. Experimental scheme of the fabrication and annealing processes of the confined PS nanotubes in the nanopores of AAO templates. At first, a PS solution is infiltrated into the nanopores of an AAO template via capillary force. After the solvents are dried, polymer nanotubes are formed in the nanopores of the AAO template. The samples are then annealed at different temperatures and times.

EXPERIMENTAL SECTION

Materials. PS with a weight-average molecular weight of 100 kg/mol (PDI = 1.06) was purchased from Polymer Source, Inc. Toluene and sodium hydroxide (NaOH) were provided by Tedia. AAO templates (Anodisc 13) with the pore sizes of ~150–400 nm were obtained from Whatman, Ltd. Membrane filters with pore diameters of 0.1 and 0.2 μm were purchased from Millipore and Toyo Roshi Kaisha, respectively. The glass substrates were obtained from the FEA Company.

Fabrication of PS Nanotubes Using Different Polymer Concentrations. The solution-wetting method was used to infiltrate polymers into the nanopores of AAO templates for the fabrication of the PS nanotubes. At first, PS ($M_w = 100$ kg/mol) solutions with different concentrations (1, 3, 5, 10, and 20 wt %) in toluene were prepared. A drop of the PS solution was then deposited on a glass substrate, followed by placing an AAO template on top of the polymer solution. The PS solution was infiltrated into the nanopores of the AAO template via capillary force. Subsequently, the sample was dried in ambient conditions for 30 min and in a desiccator at room temperature for 3 h. Later, the sample was dried in a vacuum oven at 60 °C for 16 h to ensure the complete removal of the solvent.

Thermal Annealing Process of PS Nanotubes Confined in the Nanopores of AAO Templates. After the PS nanotubes were fabricated, the samples were thermally annealed at different temperatures and times using ovens that had been preheated to the desired temperatures. The samples were then taken out and dried in a desiccator at room temperature under vacuum for 3 h. The AAO templates of the samples were removed selectively by 5 wt % NaOH(aq) to release the confined PS nanostructures. Subsequently, the PS samples were rinsed with deionized water and filtered with membrane filters, followed by a drying process using a vacuum pump.

Structure Analysis and Characterization. The glass transition temperatures of the polymers are determined by TA Q200 differential scanning calorimetry (DSC). The polymer samples before and after annealing were characterized by JEOL JSM-7401F SEM with an accelerating voltage of 5 kV. Before the SEM measurements, the samples were coated with platinum using a JEOL JFC-1600 sputter coater at 20 mA for 50 s to increase the conductivity. The samples were also examined by JEOL-2100 transmission electron microscopy (TEM) with an accelerating voltage of 200 kV, in which the samples were placed on 400 mesh carbon-coated copper grids. Quantitative studies of the SEM and TEM data were performed using the ImageJ software.

RESULTS AND DISCUSSION

Figure 2 illustrates the experimental scheme of the fabrication and annealing processes of the confined PS nanotubes in the nanopores of AAO templates. The top-view and cross-sectional-view SEM images of the AAO templates are shown in Figure 3. From the top-view SEM images (panels a and b of Figure 3), the pore sizes of the AAO templates can be estimated to be ~150–400 nm. The cross-sectional-view SEM images (panels c and d of Figure 3) also indicate that the templates possess arrays of parallel straight nanopores with relatively smooth walls. With cross-sectional SEM images at

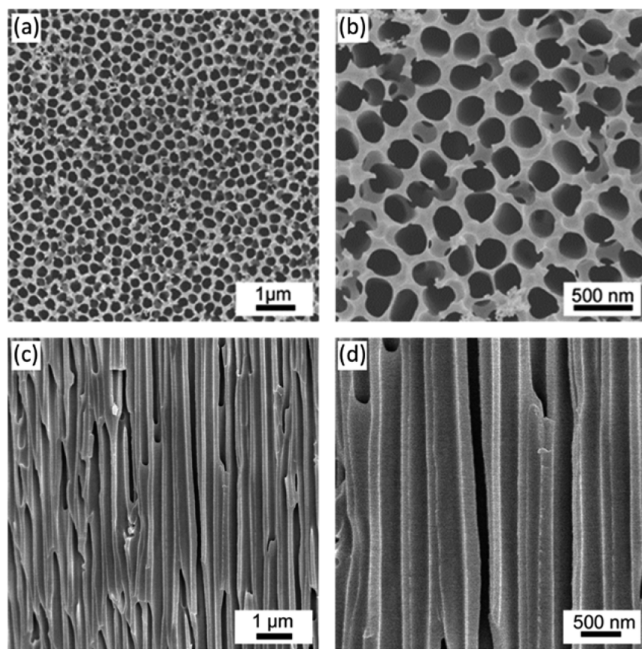


Figure 3. SEM images of AAO templates with different magnifications: (a and b) top and (c and d) cross-sectional views.

lower magnifications, the thicknesses of the AAO templates can be measured to be $\sim 60 \mu\text{m}$. The PS nanotubes are prepared by the solution-wetting method.^{30,31} Because of the high surface energy of the AAO templates, the nanopores can be easily infiltrated by the polymer solution. First, the nanopores of an AAO template are wetted by a drop of a PS solution via capillary force. After the evaporation of the solvent, the PS molecules are deposited on the walls and thin films coated in the nanopores of the AAO templates (nanotubes) are formed. The samples are then annealed thermally at different conditions. After the AAO template is removed selectively by 5 wt % NaOH(aq), the morphologies of the PS nanostructures are examined by SEM and TEM.

Here, the confined PS nanotubes are fabricated using the solution-wetting method, in which the wall thicknesses of the polymer nanotubes can be controlled by the solution concentrations and the diameters of the nanopores.^{32–34} For nanopores with the same diameters, the wall thicknesses of the polymer nanotubes increase with the solution concentrations. It has also been studied by Wendorff et al. that the wall thicknesses of the polymer nanotubes prepared by the solution-wetting method are independent of the molecular weights of the polymers.³³ To obtain the confined PS nanotubes with different wall thicknesses and diameters, PS solutions in toluene with the concentrations of 1, 3, 5, 10, and 20 wt % are used.

First, we examine the PS nanostructures before the thermal annealing processes. Panels a and b of Figure 4 show the side-view SEM images of the prepared PS nanotubes using a 5 wt % PS solution with low and high magnifications, respectively. The diameters of the PS nanotubes are ~ 150 – 400 nm , which correspond to the nanopore sizes of the AAO templates. The open-end structures of the PS nanotubes can be seen in the tilt-view image (see Figure 4c). To confirm the morphologies of the PS nanostructures further, TEM measurements are also performed. As shown in Figure 4d, the tubular structure and the wall thickness of a single PS nanotube can be observed,

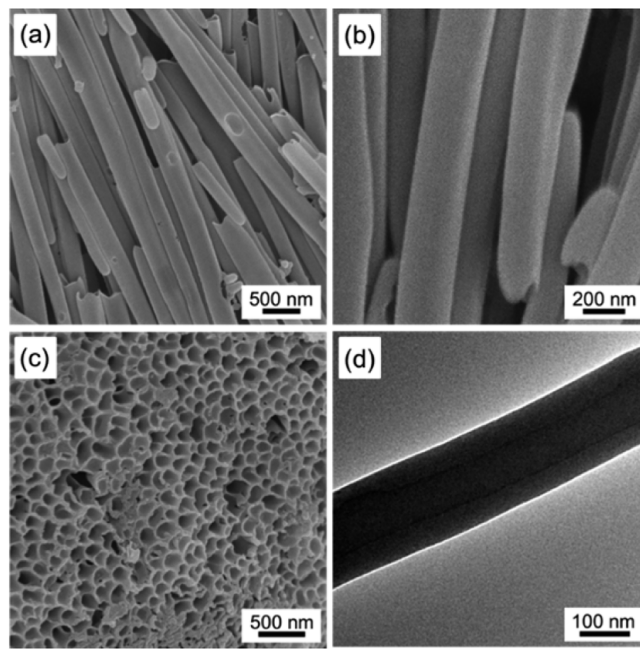


Figure 4. SEM and TEM images of PS ($M_w = 100 \text{ kg/mol}$) nanotubes fabricated by the solution-wetting method using a 5 wt % PS solution: (a and b) side-view SEM images with low and high magnifications, (c) tilt-view SEM images, and (d) TEM image. In panel d, the diameter and wall thickness of the PS nanotube are ~ 170 and $\sim 40 \text{ nm}$, respectively.

where the tube diameter and wall thickness are ~ 170 and $\sim 40 \text{ nm}$, respectively.

It has to be noted that the PS nanotubes shown in Figure 4a are not very uniform, especially in length. There are three possible reasons accounting for the non-uniformity of the fabricated PS nanotubes. First, there are some distributions of the pore sizes of the AAO templates, as shown in Figure 3. Because the shapes of the PS nanotubes replicate those of the nanopores, the size distributions of the nanopores could cause the non-uniform sizes of the PS nanotubes. Second, there are some defect regions in the AAO templates, such as the branched nanopores. The shapes of the defect regions can also be transferred to the polymer nanostructures, as shown in a branched nanotube in Figure 4a. Third, the non-uniformity of the PS nanotubes may be caused by the washing step during the experimental processes. When the PS nanotubes are formed in the nanopores of the AAO templates, the lengths of all of the nanotubes should be close to those of the AAO templates ($\sim 60 \mu\text{m}$). For the later characterization of the polymer nanostructures, the AAO templates are dissolved using 5 wt % NaOH(aq) to release the PS nanotubes. The nanotube-containing solution is then washed with deionized water several times to avoid the deposition of sodium salts on the samples. During the washing process, the PS nanotubes with high aspect ratios could be broken easily, which results in the formation of nanotubes with varied lengths. The washing process can also affect the uniformities of nanotubes from other polymers. However, for polymers such as PMMA, which possess stronger interactions to the AAO walls, more uniform nanotubes may be obtained after the washing process because of the better packing of the polymer chains.

The properties of the nanotubes are also related to the polymer concentrations for preparing the nanotubes. For example, we have observed that nanotubes prepared from

polymer solutions with lower concentrations (1 wt %) are easier to be broken than those with higher concentrations (10 or 20 wt %). Therefore, to enhance the mechanical properties and avoid the breaking of the nanotubes, polymer solutions with higher concentrations can be used. Additionally, polymers with higher molecular weights should also result in stronger nanotubes because of the higher degree of chain entanglement.

After the fabrication of the PS nanotubes confined in the nanopores of the AAO templates, the samples are annealed at temperatures above the glass-transition temperature (T_g) of PS ($T_g = 104.4$ °C, determined by DSC). Upon annealing, the tube walls of the PS nanotubes start to undulate, corresponding to structure B shown in Figure 1. With longer annealing times, the amplitude of the undulation increases and Rayleigh-instability-induced structures (structure C in Figure 1) can be formed. The Rayleigh-instability-induced structures are more stable than the nanotube structures because of the reduction of the interfacial area between air and the polymers.

The PS nanostructures annealed at different conditions are examined by SEM. Panels a and b of Figure 5 show the SEM

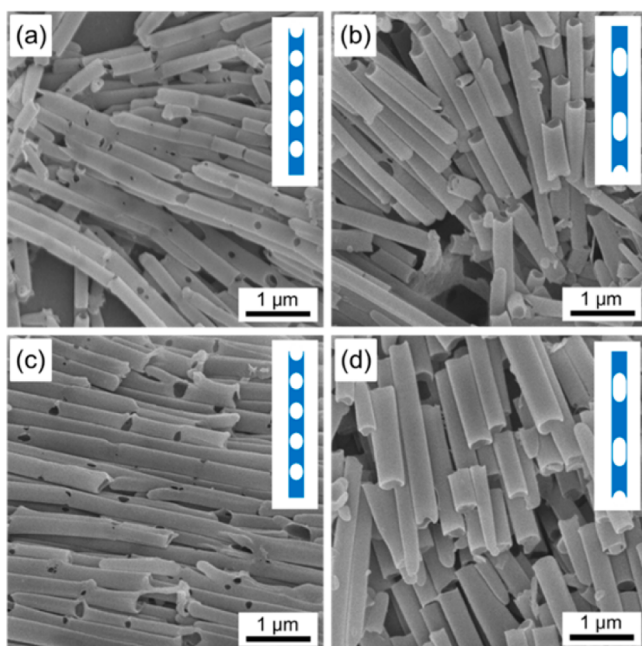


Figure 5. (a and b) SEM images of PS ($M_w = 100$ kg/mol) nanostructures prepared by a 5 wt % PS solution and annealed in the nanopores of AAO templates at 150 °C for different times: (a) 1 h and (b) 16 h. (c and d) SEM images of PS ($M_w = 100$ kg/mol) nanostructures prepared by a 20 wt % PS solution and annealed in the nanopores of AAO templates at 150 °C for different times: (c) 0.5 h and (d) 24 h. The morphologies of the polymer nanostructures shown in panels a and c correspond to structure C illustrated in Figure 1. The morphologies of the polymer nanostructures shown in panels b and d correspond to structure D illustrated in Figure 1.

images of the PS nanostructures by annealing the PS nanotubes prepared using a 5 wt % polymer solution. After annealing at 150 °C for 1 h, the nanotubes transform to the Rayleigh-instability-induced structures (structure C in Figure 1), as shown in Figure 5a. The darker areas in the SEM image indicate the locations of the air bubbles, which are covered by thin PS films. Many regions of the thin films covering the air bubbles are destroyed by the electron beam during the SEM examination, revealing the locations of the air bubbles. After

annealing at 150 °C for a longer time (16 h), the nanostructures transform further to the nanorod structures (structure D in Figure 1), as shown in Figure 5b. For the nanotubes prepared using a 20 wt % polymer solution, similar morphology transformation can also be observed, as shown in panels c and d of Figure 5. In Figure 5, most regions of PS thin films covering the air bubbles are destroyed by electron beams. To show the thin films covering the air bubbles more clearly, TEM measurements on the samples of nanorod structures are performed. Figure S2 of the Supporting Information shows the TEM image of a sample of nanorod structures that are prepared by a 20 wt % PS ($M_w = 100$ kg/mol) solution and annealed in the nanopores of AAO templates at 140 °C for 2 h, where a thin film with a thickness of ~10 nm can be observed.

From the SEM results, we find that polymer nanostructures with different morphologies can be obtained at different annealing conditions. To clarify the relationships, morphology diagrams at different annealing conditions are constructed. Figure 6 shows the morphology diagrams of the polymer nanotubes prepared from a 1 wt % PS solution. The undulated structures that correspond to structure B in Figure 1 should appear between the nanotube structures and instability structures and are not displayed in the morphology diagrams. Interestingly, similar morphology diagrams are observed using the samples prepared from other polymer concentrations (3, 5, 10, and 20 wt %), indicating that the transformation kinetics are not affected by the wall thicknesses of the PS nanotubes at the same pore diameters. This result also implies that the segmental dynamics of polymer chains in thin films of different thicknesses are unchanged. The weight-average molecular weight (M_w) of PS used in this work is 100 kg/mol, with a polydispersity of 1.06. Under this molecular weight range, the radius of gyration (R_g) is ~9 nm. Therefore, the thicknesses of the polymer nanotubes could be smaller than the range of $2R_g$ (~18 nm) when the concentration is low (3 wt % or lower). It is surprising to see that the mobilities of the polymer chains in the ultrathin films are the same as those in thicker films or bulk films. Further experiments might be necessary in the future to confirm the observation of the unchanged mobilities of polymer chains in ultrathin films.

The results of the transformation kinetics may also be related to the glass transition behaviors of polymers confined in cylindrical nanopores. Recently, many researchers have studied the glass transition behaviors of polymer chains confined in the nanopores of AAO templates. For example, Mijangos et al. have performed dielectric spectroscopy experiments to observe the relaxation behavior of PMMA confined in the nanopores of AAO templates.³⁵ They found that the effects of interfacial interactions dominate at smaller pore diameters, while the effects of confinement play a more important role at larger pore diameters. Another example is given by Xue et al., who observed two distinct glass transition temperatures (T_g) of PMMA confined in the nanopores of AAO templates and proposed a two-layer model.³⁶ The authors described a strongly constrained interfacial layer with an increased T_g and a core with a decreased T_g compared to that of the bulk polymer.

In this work, we observe that the transformation kinetics are not affected by the wall thicknesses of the PS nanotubes at the same pore diameters, which implies unchanged mobilities of the polymer chains in the thin films. The unchanged mobilities of the polymer chains may be related to the free surface area and the interfacial interactions between the polymers and the substrates. The reduction of the mobilities near the substrate

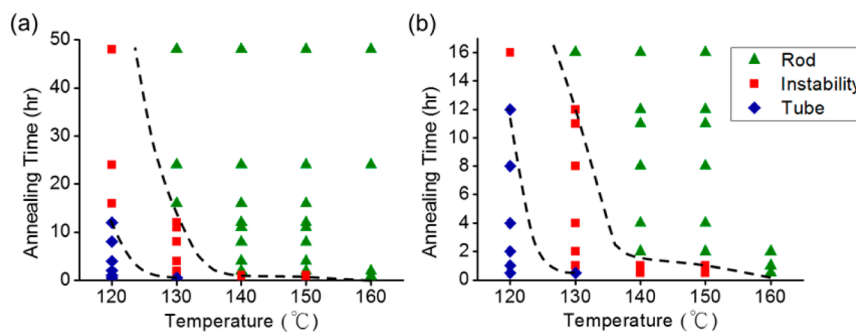


Figure 6. (a and b) Morphology diagrams of PS nanostructures annealed at different temperatures and times using a 1 wt % PS solution. The scale of the vertical (*y*) axis in part b is enlarged to show the transition regions better at higher temperatures. Similar morphology diagrams are obtained using the samples prepared from other polymer concentrations (3, 5, 10, and 20 wt %). The solid blue diamond represents the nanotube structures (structure A in Figure 1). The solid red square represents the Rayleigh-instability-induced structures (structure C in Figure 1). The solid green triangle represents the nanorod structures (structure D in Figure 1). To demarcate the different morphologies, black dash lines are drawn to guide the eye.

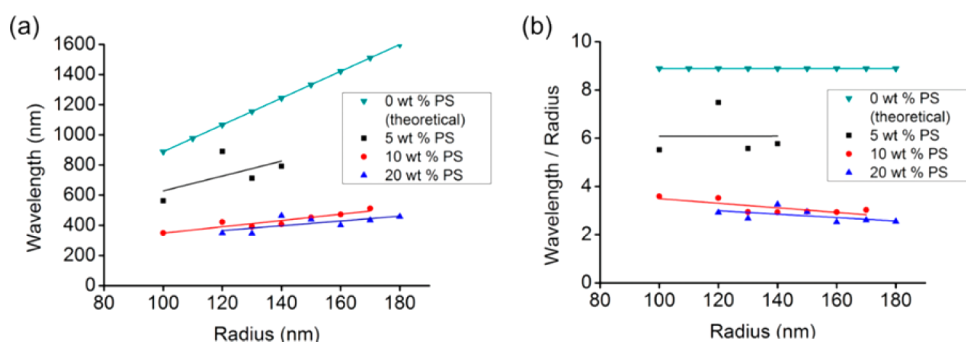


Figure 7. (a) Plot of the undulation wavelength versus the radius of the nanopores of the AAO templates. (b) Plot of the wavelength divided by the radius of the nanopores of the AAO templates versus the radius.

(increase in T_g) may balance the enhanced mobilities near the film surface (decrease in T_g). It has to be noted that the free surfaces present in our nanotube systems are absent in the nanorod systems performed by others.^{35,36} Therefore, the effect of the free surface may cause the enhanced mobilities near the film surface (decrease in T_g) that could balance the effect of the interfacial interactions between the polymers and the substrates (increase in T_g). To study the effects of the free surfaces and the interfacial interactions further, we plan to fabricate PMMA nanotubes. We expect that the stronger interactions between PMMA and AAO walls than those between PS and AAO walls may result in slower transformation kinetics of polymer films at thinner film thicknesses.

To clarify the transformation process, here, we also perform quantitative studies by measuring the distances between the air bubbles in the Rayleigh-instability-induced structures (structure C in Figure 1). The distances are assumed to be equal to the undulation wavelengths in the undulated structures (structure B in Figure 1). To reflect the transformation better visually, we can consider the system as an air cylinder surrounded by a polymer matrix. Therefore, the undulation wavelength (λ) should be determined by the radii (a) of the air cylinders, instead of the radii of the polymer nanotubes (b), according to the original theory of the Rayleigh instability.

$$\lambda = 2\pi\sqrt{2}a \quad (1)$$

Figure 7a is the plot of the undulation wavelength (λ) versus the radius (b) of the nanopores of the AAO template at different polymer concentrations. The data points are grouped using intervals of different radii. For example, the radii

between 115 and 125 nm are grouped into the class of 120 nm, while the radii between 125 and 135 nm are grouped into the class of 130 nm. At 0 wt %, which is inaccessible experimentally, the radii of the air cylinder (a) are equal to the radii of the nanopores (b). Therefore, the theoretical values (for 0 wt %) can be obtained using eq 1, as shown as the green triangles in Figure 7. Figure 7b shows the plot of the wavelength divided by the radius of the nanopores of the AAO templates versus the radius to eliminate the effect of different radii. The theoretical value (for 0 wt %) of the wavelength divided by the radius of the nanopores is a constant.

$$\lambda/b = \lambda/a = 2\pi\sqrt{2} \approx 8.89 \quad (\text{for } 0 \text{ wt \%}) \quad (2)$$

As shown in both Figures 7a and 7b, the experimental data are closer to the theoretical data (for 0 wt %) as the polymer concentration decreases. With lower polymer concentrations, the wall thicknesses of the polymer nanotubes decrease and the radii of the air cylinders increase at a given pore diameter, resulting in smaller discrepancies of the data from the theoretical values (for 0 wt %). The data shown in Figure 7 are obtained from polymer solutions with the concentrations of 5, 10, and 20 wt %. For samples with concentrations lower than 5 wt %, the data are not shown because the mechanical properties of the nanostructures are weaker and the distances between the air bubbles are difficult to be measured.

CONCLUSION

We study the Rayleigh-instability-type transformation of confined PS nanotubes in the nanopores of AAO templates.

The PS nanotubes with different wall thicknesses are first prepared using polymer solutions with various concentrations. After annealing, PS nanostructures with different morphologies can be obtained, depending upon the annealing temperatures and times. Similar morphology diagrams are obtained from the PS nanotubes prepared from different concentrations, indicating that the transformation processes are not affected by the wall thicknesses. The relationship between the undulation wavelength and the radius of the nanopores of the AAO template is also established. With lower polymer concentrations, the wall thicknesses of the polymer nanotubes decrease at a given pore diameter, resulting in smaller discrepancies of the data from the theoretical values at 0 wt %.

■ ASSOCIATED CONTENT

S Supporting Information

Introduction of the Rayleigh instability and the TEM image of PS nanorods. This material is available free of charge via the Internet at <http://pubs.acs.org>.

■ AUTHOR INFORMATION

Corresponding Author

*Telephone: +86-3-5731631. E-mail: jtchen@mail.nctu.edu.tw.

Notes

The authors declare no competing financial interest.

■ ACKNOWLEDGMENTS

This work was supported by the Ministry of Science and Technology of the Republic of China.

■ REFERENCES

- Martin, C. R. Template synthesis of electronically conductive polymer nanostructures. *Acc. Chem. Res.* **1995**, *28* (2), 61–68.
- Frenot, A.; Chronakis, I. S. Polymer nanofibers assembled by electrospinning. *Curr. Opin. Colloid Interface Sci.* **2003**, *8* (1), 64–75.
- Mora-Huertas, C. E.; Fessi, H.; Elaissari, A. Polymer-based nanocapsules for drug delivery. *Int. J. Pharm.* **2010**, *385* (1–2), 113–142.
- Jang, J.; Springer, V. Conducting polymer nanomaterials and their applications. *Emissive Materials: Nanomaterials*; Springer-Verlag: Berlin, Germany, 2006; Vol. 199, pp 189–259.
- Chen, J. T.; Hsu, C. S. Conjugated polymer nanostructures for organic solar cell applications. *Polym. Chem.* **2011**, *2* (12), 2707–2722.
- Martin, C. R. Nanomaterials—A membrane-based synthetic approach. *Science* **1994**, *266* (5193), 1961–1966.
- Martin, J.; Maiz, J.; Sacristan, J.; Mijangos, C. Tailored polymer-based nanorods and nanotubes by “template synthesis”: From preparation to applications. *Polymer* **2012**, *53* (6), 1149–1166.
- Steinhart, M.; Wendorff, J. H.; Greiner, A.; Wehrspohn, R. B.; Nielsch, K.; Schilling, J.; Choi, J.; Gosele, U. Polymer nanotubes by wetting of ordered porous templates. *Science* **2002**, *296* (5575), 1997–1997.
- Steinhart, M.; Wehrspohn, R. B.; Gosele, U.; Wendorff, J. H. Nanotubes by template wetting: A modular assembly system. *Angew. Chem., Int. Ed.* **2004**, *43* (11), 1334–1344.
- Haberkorn, N.; Lechmann, M. C.; Sohn, B. H.; Char, K.; Gutmann, J. S.; Theato, P. Templated organic and hybrid materials for optoelectronic applications. *Macromol. Rapid Commun.* **2009**, *30* (14), 1146–1166.
- Chen, J. T.; Lee, C. W.; Chi, M. H.; Yao, I. C. Solvent-annealing-induced nanowetting in templates: Towards tailored polymer nanostructures. *Macromol. Rapid Commun.* **2013**, *34* (4), 348–354.
- Reid, D. K.; Ehlinger, B. A.; Shao, L.; Lutkenhaus, J. L. Crystallization and orientation of isotactic poly(propylene) in cylindrical nanopores. *J. Polym. Sci., Part B: Polym. Phys.* **2014**, *52* (21), 1412–1419.
- Michell, R. M.; Blaszczyk-Lezak, I.; Mijangos, C.; Muller, A. J. Confined crystallization of polymers within anodic aluminum oxide templates. *J. Polym. Sci., Part B: Polym. Phys.* **2014**, *52* (18), 1179–1194.
- Jani, A. M. M.; Losic, D.; Voelcker, N. H. Nanoporous anodic aluminium oxide: Advances in surface engineering and emerging applications. *Prog. Mater. Sci.* **2013**, *58* (5), 636–704.
- Lee, W.; Park, S. J. Porous anodic aluminum oxide: Anodization and templated synthesis of functional nanostructures. *Chem. Rev.* **2014**, *114* (15), 7487–7556.
- Poinern, G. E. J.; Ali, N.; Fawcett, D. Progress in nano-engineered anodic aluminum oxide membrane development. *Materials* **2011**, *4* (3), 487–526.
- Nielsch, K.; Choi, J.; Schwirn, K.; Wehrspohn, R. B.; Gosele, U. Self-ordering regimes of porous alumina: The 10% porosity rule. *Nano Lett.* **2002**, *2* (7), 677–680.
- Li, A. P.; Muller, F.; Birner, A.; Nielsch, K.; Gosele, U. Hexagonal pore arrays with a 50–420 nm interpore distance formed by self-organization in anodic alumina. *J. Appl. Phys.* **1998**, *84* (11), 6023–6026.
- Jessensky, O.; Muller, F.; Gosele, U. Self-organized formation of hexagonal pore arrays in anodic alumina. *Appl. Phys. Lett.* **1998**, *72* (10), 1173–1175.
- Chen, J. T.; Zhang, M. F.; Russell, T. P. Instabilities in nanoporous media. *Nano Lett.* **2007**, *7* (1), 183–187.
- Chen, D.; Chen, J. T.; Glogowski, E.; Emrick, T.; Russell, T. P. Thin film instabilities in blends under cylindrical confinement. *Macromol. Rapid Commun.* **2009**, *30* (4–5), 377–383.
- Tsai, C. C.; Chen, J. T. Rayleigh instability in polymer thin films coated in the nanopores of anodic aluminum oxide templates. *Langmuir* **2014**, *30* (1), 387–393.
- Eggers, J.; Villermaux, E. Physics of liquid jets. *Rep. Prog. Phys.* **2008**, *71* (3), 036601.
- Plateau, J. *Transl. Annu. Rep. Smithsonian Inst.* **1873**, 1863–1866.
- Nichols, F. A.; Ilins, W. W. Surface- (interface-) and volume-diffusion contribution to morphological changes driven by capillarity. *Trans. Metall. Soc.* **1965**, *233*, 1840–1848.
- Rayleigh, L. On the instability of jets. *Proc. London Math. Soc.* **1878**, *10*, 4–13.
- Park, H.; Russell, T. P.; Park, S. Spatial control of dewetting: Highly ordered Teflon nanospheres. *J. Colloid Interface Sci.* **2010**, *348* (2), 416–423.
- Toimil-Molares, M. E.; Balogh, A. G.; Cornelius, T. W.; Neumann, R.; Trautmann, C. Fragmentation of nanowires driven by Rayleigh instability. *Appl. Phys. Lett.* **2004**, *85* (22), 5337–5339.
- Mei, S. L.; Feng, X. D.; Jin, Z. X. Fabrication of polymer nanospheres based on Rayleigh instability in capillary channels. *Macromolecules* **2011**, *44* (6), 1615–1620.
- Cepak, V. M.; Martin, C. R. Preparation of polymeric micro- and nanostructures using a template-based deposition method. *Chem. Mater.* **1999**, *11* (5), 1363–1367.
- Lee, C. W.; Wei, T. H.; Chang, C. W.; Chen, J. T. Effect of nonsolvent on the formation of polymer nanomaterials in the nanopores of anodic aluminum oxide templates. *Macromol. Rapid Commun.* **2012**, *33* (16), 1381–1387.
- Dougherty, S.; Liang, J. Core–shell polymer nanorods by a two-step template wetting process. *Nanotechnology* **2009**, *20* (29), 295301.
- Schlitt, S.; Greiner, A.; Wendorff, J. H. Cylindrical polymer nanostructures by solution template wetting. *Macromolecules* **2008**, *41* (9), 3228–3234.
- Chen, J. T.; Wei, T. H.; Chang, C. W.; Ko, H. W.; Chu, C. W.; Chi, M. H.; Tsai, C. C. Fabrication of polymer nanopeapods in the nanopores of anodic aluminum oxide templates using a double-solution wetting method. *Macromolecules* **2014**, *47* (15), 5227–5235.

(35) Blaszczyk-Lezak, I.; Hernandez, M.; Mijangos, C. One dimensional PMMA nanofibers from AAO templates. Evidence of confinement effects by dielectric and Raman analysis. *Macromolecules* **2013**, *46* (12), 4995–5002.

(36) Li, L. L.; Zhou, D. S.; Huang, D. H.; Xue, G. Double glass transition temperatures of poly(methyl methacrylate) confined in alumina nanotube templates. *Macromolecules* **2014**, *47* (1), 297–303.